



16 **Abstract**

17       The northeastern part of the North Atlantic subpolar gyre is a key passage for the  
18 Atlantic Meridional Overturning Circulation upper cell. To this day, the precise path-  
19 way and intensity of bottom currents in this area have not reached a consensus. In this  
20 study, we make use of regional high resolution numerical modeling to suggest that the  
21 main bottom current flowing south of Iceland originates from both the Faroe-Bank Chan-  
22 nel and the Iceland-Faroe Ridge (with about equal contributions) and then flows along  
23 the topographic slope centered on the  $1027.75 \text{ kg m}^{-3}$  isopycnal. When flowing over the  
24 rough topography, this bottom current generates a bottom mixed layer reaching 200 m  
25 height. We further demonstrate that many submesoscale structures are generated at the  
26 southernmost tip of the Icelandic shelf, thus spreading water masses in the open Iceland  
27 Basin. These findings have major implication in the better understanding of the trans-  
28 port of dense water masses in the North Atlantic, but also for the distribution of ben-  
29 thic species along the Icelandic shelf.

30 **Plain Language Summary**

31 Water masses formed in the Arctic Ocean overflow into the North Atlantic at the  
32 bottom of the ocean, forming the so-called upper cell of the Atlantic Meridional Over-  
33 turning Circulation (AMOC). The pathway of the currents carrying these water masses  
34 is still under debate due to a lack of observations. In this study, we discuss in details the  
35 pathway of these bottom currents in the specific area south of Iceland. We show that  
36 a steady current flows along the Icelandic continental shelf, and then divide in smaller  
37 structures when reaching the southernmost tip of Iceland. We also show that on its way,  
38 the current mixes the bottom layer of the ocean. These findings have major implication  
39 in the understanding of heat and carbon transport at depth in this area, which consti-  
40 tute an important response of the climate to anthropogenic forcing.

## 41 1 Introduction

42 The northeastern part of the North Atlantic subpolar gyre is a key part of the At-  
43 lantic Meridional Overturning Circulation (AMOC, Buckley & Marshall, 2016). Its so-  
44 called "upper cell" ventilates the upper 2 km of the Atlantic Ocean, and it transports  
45 heat and carbon at depth from the surface (Kostov et al., 2014; Marshall et al., 2014).  
46 It therefore plays a determinant role in the response of the climate to anthropogenic forc-  
47 ing (Drijfhout et al., 2012; Winton et al., 2013; Meehl et al., 2014). The main sources  
48 of dense water into the upper cell are overflows from the Nordic Seas (Lozier et al., 2019;  
49 Chafik & Rossby, 2019; Tsubouchi et al., 2021). There, intense heat loss in winter trans-  
50 forms the water into colder and denser water masses that subsequently flow southward  
51 through gaps in topography (Brakstad, Gebbie, et al., 2023).

52 While it is the crossroad of this global circulation, the region south of Iceland has  
53 been poorly studied in details (see Fig. 1a for the location of the places mentioned be-  
54 low). At this place, there is no consensus on the shape and intensity of bottom currents.  
55 Studies agree for an overall southwestward flow from the Iceland-Faroe Ridge (IFR) and  
56 the Faroe-Bank Channel (FBC) regions toward the Iceland Basin, following the Reyk-  
57 janes Ridge, see *e.g.*, Stow & Holbrook (1984); Bianchi & McCave (1999). When look-  
58 ing at it more precisely, opinions diverge a lot, due to the lack of available data in the  
59 area. Investigators sometimes only consider the IFR, the FBC, include an overflow over  
60 the Western Valley, or assume a pathway across the deep waters of the Iceland Basin,  
61 see *e.g.*, Bowles & Jahn (1983); Hansen (1985); Perkins et al. (1998); Hansen & Øster-  
62 hus (2000, 2007); Beaird et al. (2013); Logemann et al. (2013); Guo et al. (2014); Ull-  
63 gren et al. (2014); Daniault et al. (2016); Zou et al. (2017); Zhao et al. (2018); Hansen  
64 et al. (2018); Petit et al. (2019); Chafik & Rossby (2019); Semper et al. (2020); Koman  
65 et al. (2022); Brakstad, Gebbie, et al. (2023). Understanding the actual properties of lo-  
66 cal geophysical processes at depth is therefore timely. It will allow to better target fu-  
67 ture *in situ* observations aiming at quantifying water mass transport and mixing by the  
68 bottom currents, and thus better assess deep storage of anthropogenic-induced tracers.

69 Beyond this slowly-varying and averaged picture, it has been shown in the past years  
70 that small-scale processes have an important role in modulating the global ocean prop-  
71 erties. This includes submesoscale balanced currents such as Submesoscale Coherent Vor-  
72 tices (SCVs), Intrathermocline Eddies, or fronts (McWilliams, 2019). These structures

73 have been shown to be key for the global heat budget (Su et al., 2018) and the distri-  
74 bution of marine ecosystems (Lévy et al., 2018) *via* deep-reaching vertical and horizon-  
75 tal transports (Zhong & Bracco, 2013; Siegelman et al., 2020). Small-scale processes also  
76 include fine-scale vertical mixing, induced by deep-reaching currents and internal tides  
77 flowing over the topography (Vic et al., 2019; Gula et al., 2022; Polzin & McDougall, 2022).  
78 These processes are of major importance to regulate the transport of heat and biogeo-  
79 chemical tracers, and they are suggested to be a good candidate for the closing of the  
80 oceanic energy budget (Jayne, 2009; Ferrari & Wunsch, 2009; de Lavergne et al., 2022).  
81 The contribution of all these submesoscale processes in the south Icelandic dynamics has  
82 yet not been studied. However, it is likely that it plays an important role in the trans-  
83 port of water masses there. Note that the submesoscale is defined here as the scale at  
84 which processes happen on horizontal scales smaller than the average deformation ra-  
85 dius (here  $\mathcal{O}(20\text{--}30)$  km (LaCasce & Groeskamp, 2020)), and on vertical scales smaller  
86 than the bottom mixed layer (here  $\mathcal{O}(100)$  m, see section 3.2).

87 In the present paper, we discuss in details the bottom circulation south of Iceland  
88 using regional high resolution numerical modeling. In particular we discuss the shape  
89 and intensity of the bottom boundary current flowing at  $\sim 1000$  m depth along the Ice-  
90 landic shelf. This current is the connection between Nordic Seas and the northeastern  
91 part of the North Atlantic subpolar gyre. In the following, mention to the "bottom bound-  
92 ary current" refers to this current. We further show that this latter generates numer-  
93 ous submesoscale features on its path and where it overshoots. This processes are shown  
94 to be of importance for the distribution of water masses in the area. In section 2 we present  
95 the methods used to investigate these processes. In section 3 we present the analysis of  
96 the numerical simulations. In section 4 we discuss and conclude on our results.

## 2 Methods

### 2.1 Numerical simulation of the North Atlantic

We use outputs of a realistic simulation of the North Atlantic Subpolar Gyre, already used and validated in previous studies, *e.g.*, Le Corre, Gula, Smilenova, & Houper (2019); Le Corre, Gula, & Treguier (2019); de Marez & Le Corre (n.d.); Smilenova et al. (n.d.); de Marez et al. (2021); Wang et al. (2022). It is performed using the Coastal and Regional Ocean COmmunity model (CROCO, Shchepetkin & McWilliams, 2005). This model solves the hydrostatic primitive equations using the full equation of state for seawater (Shchepetkin & McWilliams, 2011). The horizontal advection terms for tracers and momentum are discretized with third-order upwind advection schemes (UP3), see *e.g.* Klein et al. (2008) for a further description. This parameterization considers implicit dissipation and it damps dispersive errors.

A one-way nesting approach is used. A first simulation of the whole North Atlantic is implemented with a  $\Delta x \sim 6$  km horizontal resolution and 50 topography-following levels, such that mesoscale eddies are reasonably well resolved. It is initialized and forced at boundaries with the SODA dataset (Carton & Giese, 2008). At the surface, the forcing is obtained from the daily ERA-INTERIM dataset (Dee et al., 2011). The bathymetry is constructed from the SRTM30 PLUS dataset (Becker et al., 2009). Then, this simulation is used as boundary forcing and initialization for a second —child— simulation in the Subpolar region, with  $\Delta x \sim 2$  km horizontal resolution and 80 topography-following levels. This higher resolution resolves small scale bathymetric features. In particular, it allows an accurate description of the FBC and the IFR.

We make use of this high resolution simulation in the present study, for the period 2002-2009 (after a 2-years spin up). Reference to time averaged quantities over this period are denoted  $\langle \cdot \rangle_t$ . The simulation has already been thoroughly validated by Le Corre, Gula, & Treguier (2019) in the Subpolar Gyre, and at the large scale. In our domain of interest, a slight average temperature and salinity offset is seen in the whole water column (constant throughout depth). However, it does not affect the average stratification (see Fig. 2c,d) which is here the main parameter for the study of the dynamical processes. For further details, we refer the reader to Le Corre, Gula, & Treguier (2019)'s description and validation of the simulation, and their Fig. 1 that presents the simulation domain.

## 129 **2.2 Particulate advection simulations**

130 We perform three offline particle advection simulations, using the velocity field from  
131 the numerical simulation on the  $1027.75 \text{ kg m}^{-3}$  isopycnal, implementing the set of python  
132 classes Parcels (Probably A Really Computationally Efficient Lagrangian Simulator). This  
133 tool has been widely used in the past few years and it is fully described in Lange & van  
134 Sebille (2017), Delandmeter & van Sebille (2019), and in references therein. The three  
135 simulations are designed such that they all are one year long. We arbitrarily chose the  
136 year 2005 of the CROCO simulation for the currents.

## 137 **2.3 *in situ* data**

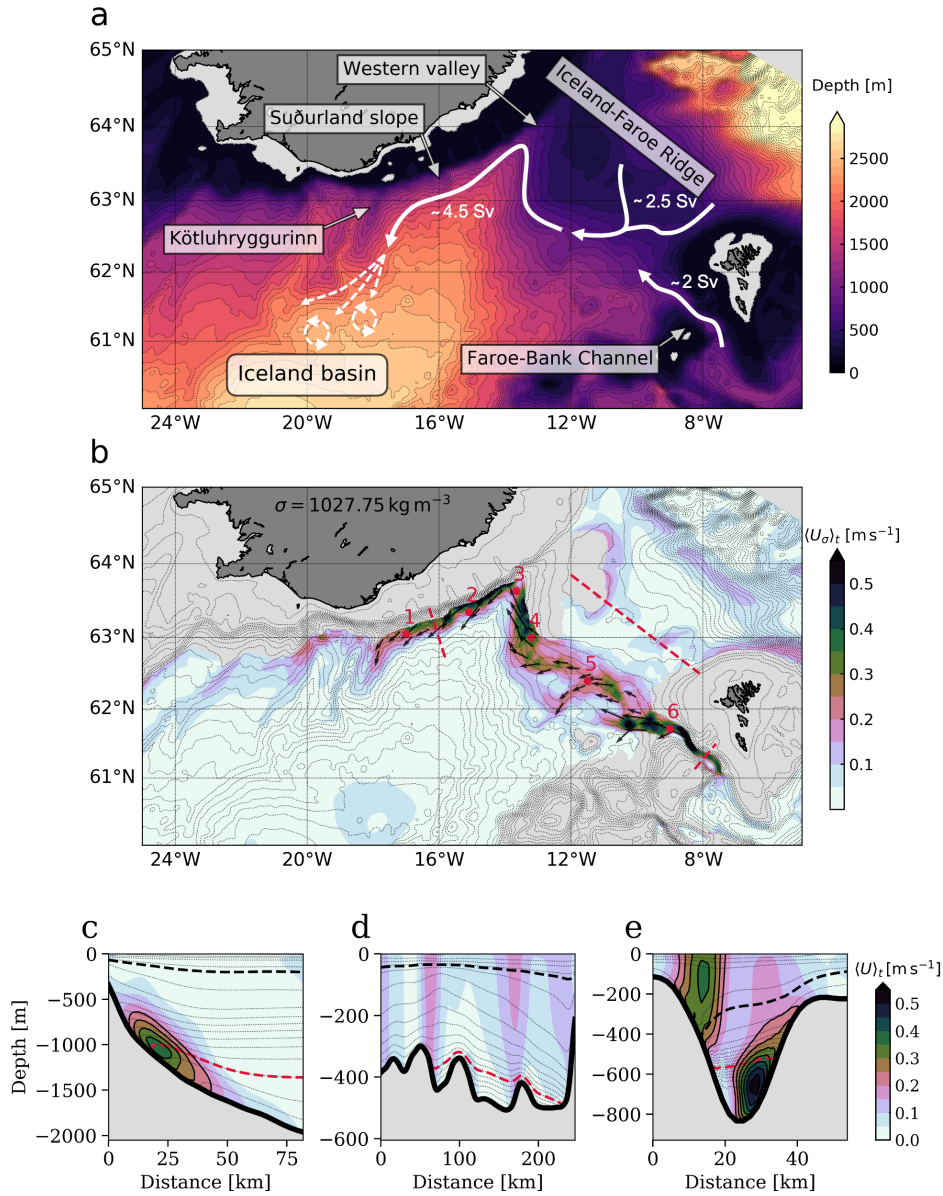
138 The data used for validation and comparison was obtained from SeaDataNet and  
139 the Norwegian Marine Data Center (Brakstad, Våge, et al., 2023) for the region south-  
140 east of Iceland, corresponding to 80 CTD profiles from 1996 until 2019 covering the 4  
141 seasons. Most of the profiles were uploaded to these open source databases by the Hy-  
142 drography Observational Programme carried out by the Icelandic Marine and Freshwa-  
143 ter Research Institute (Ólafsdóttir et al., 2020). The CTD profiles were used to validate  
144 the simulation at the virtual location of  $13.7^\circ\text{W}$  and  $63.6^\circ\text{N}$  (Stokksnes 5), shown in Fig.  
145 1b as the point labeled 3.

146

### 3 Results

147

#### 3.1 General description of the bottom current



148

**Figure 1.** a: Region of interest, bathymetry, and schematic path of the bottom current; white

149

numbers indicate the transport through the three sections shown in panels c,d,e. b: Velocity

150

norm on the  $1027.75 \text{ kg m}^{-3}$  isopycnal; position of sections shown in panels c,d,e, position of

151

profiles shown in Fig. 2, and bathymetry (thin black lines). c,d,e: Vertical sections of the velocity

152

norm and isopycnals (thin dashed every  $0.05 \text{ kg m}^{-3}$ , red dashed  $1027.75 \text{ kg m}^{-3}$ , and thick

153

dashed  $\sigma_{\text{top}} = 1027.3 \text{ kg m}^{-3}$ ).

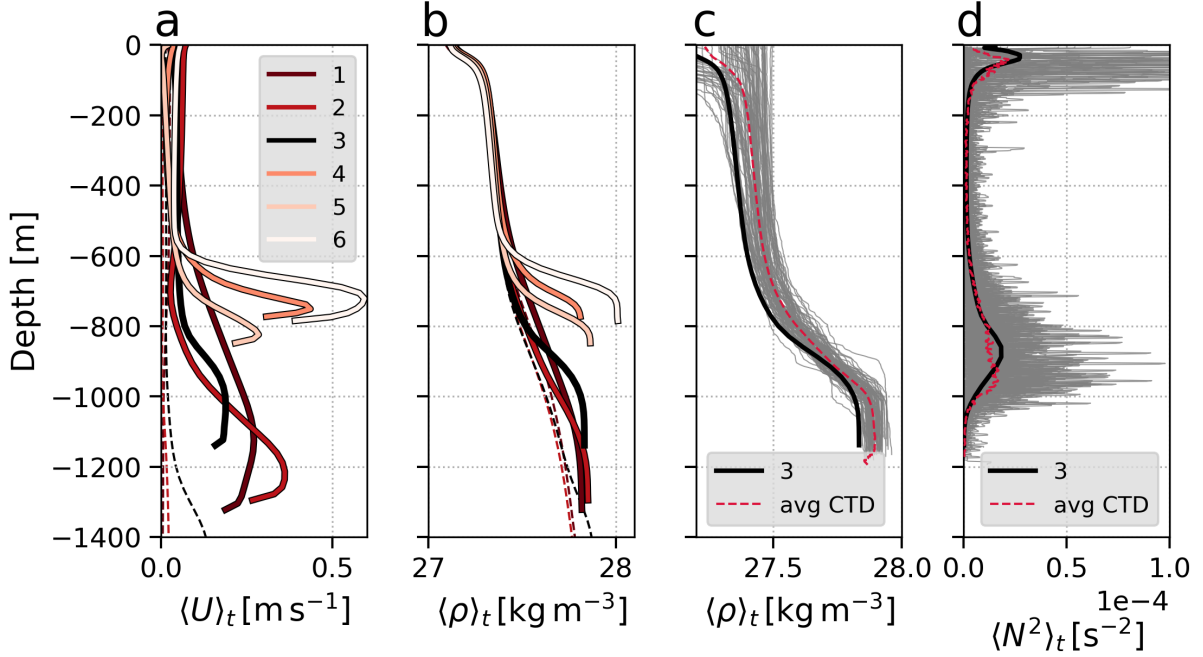
154 Time-averaged simulation outputs show that the bottom boundary current orig-  
 155 inates from two branches at the northeast boundary of the Iceland Basin. A first branch  
 156 consists of a northwestward flow coming from the FBC. There, an intense current with  
 157 average maximum velocity of  $0.53 \text{ m s}^{-1}$  located below 500 m depth flows along the north-  
 158 ern slope of the narrow channel, see Fig. 1b,e. The transport in this channel has been  
 159 shown in previous studies to be about 2 Sv (Hansen & Østerhus, 2007; Hansen et al.,  
 160 2016). We determine that this transport is satisfied when integrating the crossing cur-  
 161 rent between the  $\sigma_{\text{top}} = 1027.3 \text{ kg m}^{-3}$  isopycnal and the bottom. A second branch con-  
 162 sists of a southwestward flow coming from the IFR. There, two weak currents at  $\sim 11^\circ\text{W}$   
 163 and  $\sim 9^\circ\text{W}$  flow over the ridge. The average maximum velocity of  $0.19 \text{ m s}^{-1}$  at the bot-  
 164 tom is seen at the western most location, see Fig. 1b,d. The crossing overflow transport  
 165 between  $\sigma_{\text{top}}$  and the bottom is about 2.5 Sv, larger than the FBC transport because  
 166 of the wider section.

167 When entering the Iceland Basin, the bottom boundary current stabilizes around  
 168 the  $1027.75 \text{ kg m}^{-3}$  isopycnal, see Fig. 1b. It flows northward, constrained along the con-  
 169 tinental shelf. When reaching the Western Valley, it retroreflects following the topogra-  
 170 phy. It then flows southwestward along the continental shelf south of Iceland, namely  
 171 Suðurland slope, after the name of the Icelandic southern lands. The flow is very well  
 172 marked along the slope, with average maximum velocity of  $0.38 \text{ m s}^{-1}$  on the  $1027.75 \text{ kg m}^{-3}$   
 173 isopycnal, see Fig. 1c. This finding justifies the choice of this particular isopycnal for the  
 174 further investigation of the current made in this study. The transport induced by the  
 175 current between  $\sigma_{\text{top}}$  and the bottom is about 4.5 Sv, thus satisfying the mass conser-  
 176 vation from overflows to the Suðurland slope.

177 Finally, the current overshoots at a submarine cape located  $\sim 18^\circ\text{W}, 62.5^\circ\text{N}$ . It is  
 178 called Kötluhryggurinn, "the Katla ridge", after the Katla volcano south of Iceland (Shor,  
 179 1980). A slight part of the current overflows west over Kötluhryggurinn, creating weak  
 180 branches of current further west, see Fig. 1b. Further examination of the current using  
 181 particle advection simulations show that these branches have few impact (section 3.3).  
 182 Note that neither seasonal nor inter-annual variability of the bottom boundary current  
 183 position/intensity/depth are noticed (not shown), thus justifying the use of 7-years over-  
 184 all time averages.

185

## 3.2 Vertical variations and mixing at the bottom



186 **Figure 2.** a (resp. b): Time-averaged velocity norm (resp. potential density) profiles at the  
 187 locations shown in Fig. 1b; thin dashed profiles show profiles  $\sim 50$  km off-shore of the same-color  
 188 profiles. c (resp. d): Comparison of potential density (resp. Brunt-Väisälä frequency) profiles  
 189 between simulation (thick black) and CTD station (thin gray and thick dashed red) at location 3  
 190 (Fig. 1).

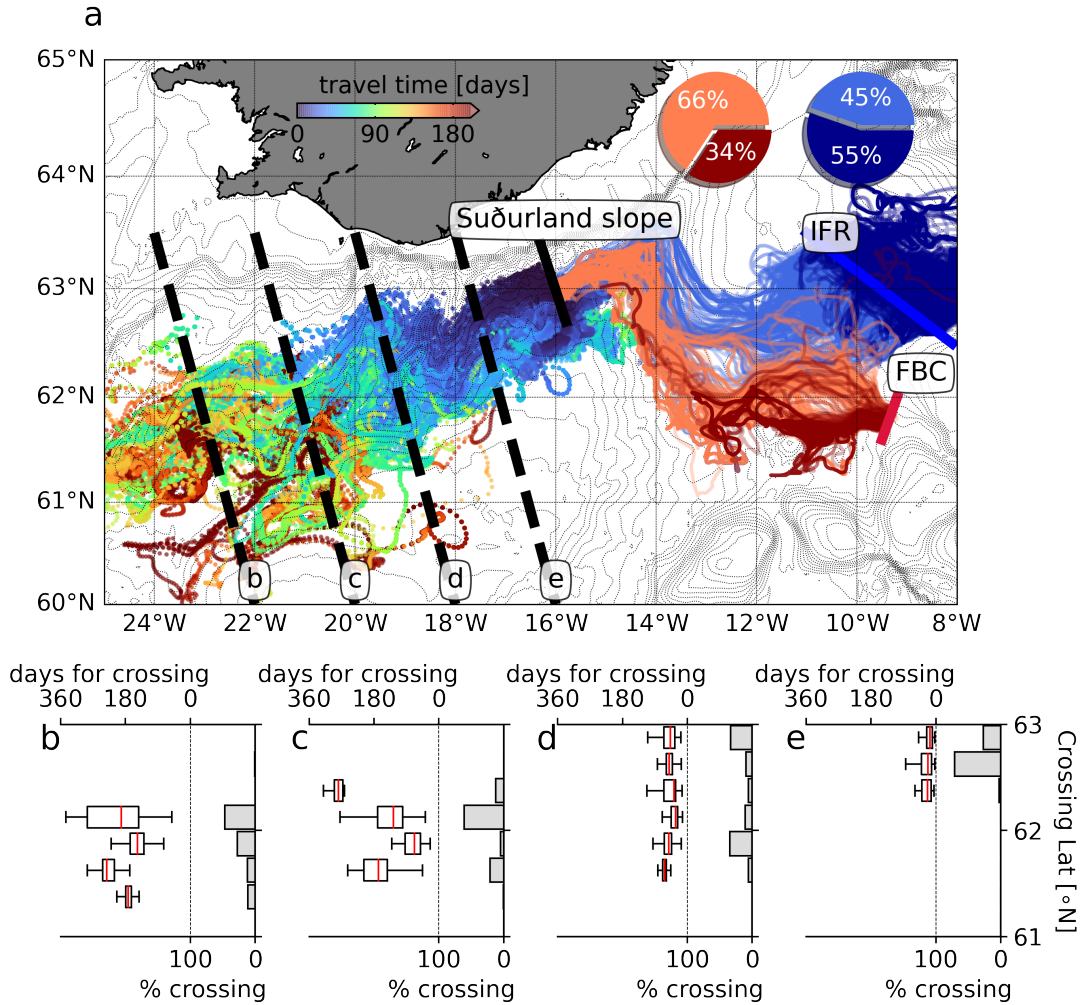
191 Along its path from the FBC to the Suðurland slope, the current has a Gaussian-  
 192 like vertical distribution, with average maximum velocity varying between  $\sim 0.2$  and  $\sim 0.6$   $\text{m s}^{-1}$ ,  
 193 and average thickness varying between  $\sim 100$  m and  $\sim 500$  m, see Fig. 2a. It dives from  
 194  $\sim 700$  m depth at the FBC mouth (profile 6) to  $\sim 1200$  m depth at Kötluhyggurinn (pro-  
 195 file 1).

196 A marked Bottom Mixed Layer (BML) is observed along the current path, see Fig.  
 197 2b,c,d, and is confirmed by 24 years of *in situ* data. This BML is less than 50 m thick  
 198 at the FBC mouth. It then becomes thicker along the IFR reaching over 200 m in the  
 199 Western Valley and along the Suðurland slope. The profile 3 position coincides with the  
 200 position of CTD casts performed during a 24 years period in the Western Valley (Stokksness  
 201 5, Ólafsdóttir et al., 2020). Average vertical profile of potential density from the simu-  
 202 lation matches with *in situ* observations. The slight offset in density is homogeneous on

203 the vertical and is mainly due to a  $\sim 0.5^\circ\text{C}$  temperature offset. Nevertheless, this does  
204 not change the dynamics as the stratification ( $N^2$ ) closely matches thus proving the oc-  
205 currence of this deep BML in the current path, and additionally validating one of the  
206 main feature of the simulated current.

207 The evolution of this BML suggest the combination of frictional and arrested bot-  
208 tom Ekman layers (Brink & Lentz, 2010). The FBC is a narrow-steep-smooth channel  
209 which allows the BML to be tightly confined ( $\sim 10$  km) against the slope; there, the ve-  
210 locity is maximum and the density contrast between the BML and the interior is also  
211 the greatest. This bottom boundary current remains confined to the slope throughout  
212 the path presented here. First evidence is that this BML is not seen  $\sim 50$  km off-shore,  
213 outside of the current path, see Fig. 2b. Along the path the BML thickness increases  
214 coincidentally with the increase in roughness on bottom topography just after the Suðurland  
215 slope, which is most likely due to submesoscale viscous processes happening at the bot-  
216 tom, when the current flows over the topography (Polzin et al., 2021).

### 3.3 The faith and spreading of carried waters



218 **Figure 3.** a: Trajectories of particles released from the IFR (blue), the FBC (red), and the  
 219 Suðurland slope (rainbow color that indicates the travel time) sections; darker blue (resp. red)  
 220 show trajectories of particles released from the IFR (resp. FBC) location that dit not cross the  
 221 Suðurland slope section; for clarity only 1 out of 4 trajectory is shown; pie charts indicate the  
 222 percentage of trajectories that crossed the Suðurland slope section when released from either  
 223 the IFR or the FBC locations; black dashed lines indicate the sections used to compute the his-  
 224 tograms shown in bottom panels. b,c,d,e: Percentage of particles crossing the sections shown in  
 225 panel a, and time for the crossing, as a function of latitude.

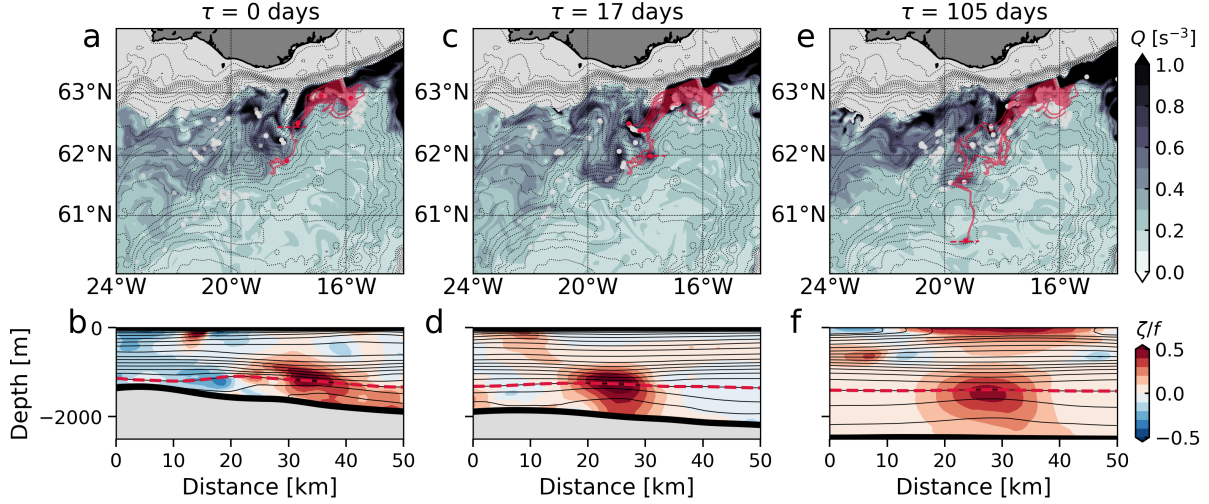
226 Two first particle advection simulations confirm that the bottom current originates  
 227 from both the IFR and the FBC overflows. A total of 6 (resp. 26) particles are released  
 228 everyday during 300 days along a straight line located in the FBC (resp. on the IFR)  
 229 on the  $1027.75 \text{ kg m}^{-3}$  isopycnal, see Fig. 3a. Remarkably, all particles overflowing in the

230 Iceland Basin eventually get trapped along a very narrow path along the Suðurland slope.  
231 We then measure the number of particles from each simulation that cross a section per-  
232 pendicular to the Suðurland slope, see Fig. 3a. Some particles do not reach this region  
233 at the end of the simulations (34% and 55%); those particles were either advected too  
234 slowly or flowing east of the IFR (see dark blue and dark red trajectories in Fig. 3a).  
235 Nevertheless, when particles released at both locations get trapped in the bottom cur-  
236 rent they always travel north toward the Western Valley before retroreflecting to the west  
237 and crossing the Suðurland slope section. Note that an additional backward advection  
238 simulation described in Supplementary Information confirms these findings.

239 Then, a third simulation is designed in which 15 particles are released everyday dur-  
240 ing a year along a straight line perpendicular to the the Suðurland slope on the  $1027.75 \text{ kg m}^{-3}$   
241 isopycnal, *i.e.*, the same section as the one mentioned previously, see Fig. 3a. Particle  
242 trajectories from this simulation shows that when reaching Kötluhryggurinn, the waters  
243 carried by the bottom current spread out in the Iceland Basin. We measure the latitude  
244 and the travel time at which particles cross four different sections, parallel to the launch-  
245 ing section, each spaced of  $2^\circ$  in the longitudinal direction, see Fig. 3. Particles cross the  
246 first section (e) in a few weeks and are concentrated north of  $62.5^\circ \text{N}$ , see Fig. 3e. Af-  
247 ter passing Kötluhryggurinn, and as they travel southwestward, they detach from the  
248 continental slope, and they cross sections with a large spreading, see Fig. 3b,c,d. Par-  
249 ticles crossing section b are all located south of  $62.25^\circ \text{N}$ , and some particles even crossed  
250 the 60th parallel North. The spreading is due to turbulent processes, with short time scales,  
251 as revealed by the large standard deviations of crossing times. This is also highlighted  
252 by the fact that particles are advected by a flow with high values of relative vorticity.  
253 In particular, most of the particles have a cyclonic vorticity reaching  $\zeta/f > 0.5$  due to  
254 the generation of submesoscale structures at Kötluhryggurinn (see Fig. 2 of Supplemen-  
255 tary information). These processes are described in the following section.

256

### 3.4 Submesoscale generation at Kötluhryggurinn



257 **Figure 4.** a,c,e: Snapshots of Potential Vorticity (divided by  $10^9$ ) on the  $1027.75 \text{ kg m}^{-3}$   
 258 isopycnal; position of particles trapped (resp. don't trapped) by the SCV at  $\tau = 105$  days is  
 259 shown by the red (resp. white) dots. b,d,e: vertical section of normalized relative vorticity at the  
 260 position shown by the red dashed lines in top panels; isopycnals are shown in thin black lines; the  
 261  $1027.75 \text{ kg m}^{-3}$  isopycnal is shown by the thick dashed red line.

262 Water masses are spread out in the Iceland Basin by submesoscale structures prop-  
 263 agating from Kötluhryggurinn. The mechanism is as follows. The bottom current flows  
 264 along the Suðurland slope, concentrated around the  $1027.75 \text{ kg m}^{-3}$  isopycnal. Viscous  
 265 interactions (parameterized in the model, see Le Corre, Gula, & Treguier (2019)) with  
 266 the topography leads to a frictional injection of Potential Vorticity (PV) on this isopy-  
 267 cnal. This in turn generates a change of sign of the cross-current PV gradient both hor-  
 268 izontally and vertically (see Fig. 3 of Supplementary Information). These are the nec-  
 269 essary conditions for Barotropic and Baroclinic instabilities to occur. This results in a  
 270 highly turbulent flow along the Suðurland slope, as reflected by the high values of Eddy  
 271 Kinetic Energy (EKE) and Eddy Available Potential Energy (EAPE) on this isopycnal  
 272 (see Fig. 3 and 4 of Supplementary Information). The flow overshooting at Kötluhryg-  
 273 gurinn thus does not follow the slope but meanders south in the Iceland Basin. Water  
 274 masses are stirred and spread out offshore by intense fronts and rapidly varying flows  
 275 with —mainly cyclonic— values of vorticity reaching  $\zeta/f > 0.5$  (see Fig. 2 of Supple-  
 276 mentary Information). Occasionally, the tongue of potential vorticity wraps onto itself,  
 277 generating cyclonic SCVs on the  $1027.75 \text{ kg m}^{-3}$  isopycnal.

278           The cyclonic SCVs generated at Kötluhryggurinn enhance the spreading of water  
279 masses. A particular event of SCV generation is shown in Fig. 4. This structure was gen-  
280 erated following the mechanism discussed in the previous paragraph. It then traveled  
281 south, hundreds of kilometers, carrying water masses offshore. At  $\tau = 105$  days (Fig.  
282 4e,f), 175 particles (out of 5464 released in total during the simulation) are trapped in  
283 its core and travel southward. This represents more than 3% of the total amount of par-  
284 ticles present along the Suðurland slope during a year, that have been spread out by this  
285 single event. Counting the number of such events is arduous because most of the time  
286 generated SCVs merge between each other making the tracking of single structures haz-  
287 ardous. Nevertheless, we report 15-20 events in the year 2005 of the simulation. This sug-  
288 gests that  $\mathcal{O}(50)\%$  of water masses present along the Suðurland slope could be spread  
289 in the basin by locally generated SCVs.

## 4 Discussion

In this study, we investigated the bottom boundary current flowing in the north of the Iceland Basin. We showed that it originates from both the Faroe-Bank Channel and the Iceland-Faroe Ridge. It then follows the topography on the  $1027.75 \text{ kg m}^{-3}$  isopycnal where it induces bottom mixing creating a large Bottom Mixed Layer. It finally overshoots at K tluhryggurinn, where submesoscale structures are generated and spread water masses in the open Iceland Basin.

In the past decades, circulation in the northern Iceland Basin has been investigated due to its role in the Atlantic Meridional Overturning Circulation, and numerous schematized views of the bottom circulation have emerged. The present paper aims at suggesting that the bottom circulation of the North Iceland basin is as schematized as in Fig. 1a, with a current coming from both the Faroe-Bank Channel and the Iceland-Faroe Ridge (with about equal contributions) and flowing along the topographic slope. More importantly, our study put forth the fact that when overshooting at K tluhryggurinn, the bottom current somehow disappears and let place to a submesoscale processes-driven spreading of the water masses in the Iceland basin, thus making obsolete the view of a current steadily flowing along the Reykjanes Ridge. In particular, a significant amount of water is spread out by locally generated cyclonic SCVs. Even if only a few *in situ* experiments succeeded in measuring SCVs with a sufficient horizontal resolution (see *e.g.*, L'H garet et al., 2016; Meunier et al., 2018; Gula et al., 2019, and references therein), only a few observations of *cyclonic* SCVs were reported (*e.g.*, Bosse et al., 2016; de Marez et al., 2020), suggesting that anticyclonic SCVs are predominant in the deep ocean. Our findings thus further suggest that K tluhryggurinn is an efficient generation spot for deep intense *cyclonic* SCVs. This result is to be confirmed by *in situ* measurements in the area to allow further analysis of these peculiar submesoscale structures.

The region described in this manuscript is of great importance for the future of the AMOC. Indeed, the dense water carried by the bottom current has enormous importance as it significantly contributes to the lower limb of the AMOC. Moreover, the winter convection there can create surface mixed layer depths over 700 m (Brakstad, Gebbie, et al., 2023), which in some regions allows the exchange of surface waters with dense bottom waters. The upper ocean in this region is warming up and IPCC projections suggest this will continue at even higher rates than other basins (Shu et al., 2022). South

322 of Iceland, the combination of deep mixed layers with warmer surface waters, and thick  
323 bottom boundary currents with cold-dense waters may exchange this excess of heat re-  
324 sulting in changes of these dense waters in a warming climate.

325 The bottom boundary current described in this study also appears to be a key phe-  
326 nomenon to sustain biological activity in the area. Indeed, the distribution of several Cold  
327 Water Coral species, in particular *Lophelia pertusa*, strongly correlates with the position  
328 of the bottom current we described (see Fig. 4 of Buhl-Mortensen et al., 2015). It has  
329 been shown in the past that the presence of benthic species, such as Cold Water Coral,  
330 is strongly correlated to the physical and chemical properties of seawater. In particular,  
331 they rely on a renew of suspended food sources and oxygenated waters, *i.e.*, feeding cur-  
332 rents (Mienis et al., 2019). The bottom current described here has the potential to act  
333 as a enhancement-nutrient-supply current. Its strong intensity efficiently renews the bot-  
334 tom water. The interaction of the current with the topography south of Iceland induces  
335 strong vertical gradients, locally enhancing vertical mixing of cold nutrient-rich bottom  
336 water to the upper layers. The bottom mixing induced by the current also enhances this  
337 water flushing, and contributes in increasing the bottom temperature, necessary condi-  
338 tion for this species to survive. This current may have implication to a broader spectrum  
339 of benthic species, but more investigation in this direction, and a better sampling of physical-  
340 biology-related quantities at the bottom is needed to pursue this question.

341 Finally, even if it is mainly speculations, it is interesting to draw the question of  
342 Kötluhryggurinn formation. Studies have discussed the fact that "The Katla Ridges are  
343 smooth features with accumulation of sediment beneath the crests in excess of 1.5 kilo-  
344 meters. Their mode of formation is inferred to result from the rapid denudation of Ice-  
345 land during the Neogene, sediment transport to the base of the slope by turbidity cur-  
346 rents and subsequent entrainment and transport southwestward by the flow of Iceland-  
347 Scotland Overflow Water." (Shor, 1980). Even if some other exchanges from the shelf  
348 into the canyons may contribute to the sediments, several sources (see *e.g.*, Bowles &  
349 Jahn, 1983), suggest that the bottom current has lead to the formation of this bathy-  
350 metric feature. Taking a step back, this suggests that the bottom current formed Kötluhryg-  
351 gurinn topographic anomaly, which in turn contributed to the generation of submesoscale  
352 at this particular place. This could be the signature of geological-timescale forced sub-  
353 mesoscale process.

## 354 **Acknowledgments**

355 C.d.M. was supported by a Queen Margrethe II's and Vigdís Finnbogadóttir's In-  
356 terdisciplinary Research Centre on Ocean, Climate and Society (ROCS) postdoctoral fel-  
357 lowship. A.R.A. was supported by ROCS. M.L.C. was supported by the French Naval  
358 Hydrographic and Oceanographic Service (SHOM) during the writing and by UBO and  
359 Région Bretagne through ISblue, Interdisciplinary graduate school for the blue planet  
360 (ANR-17-EURE-0015) and co-funded by a grant from the French government under the  
361 program "Investissements d'Avenir" during the setup and run of the experiment. Sim-  
362 ulations were performed using the HPC facilities DATARMOR of 'Pôle de Calcul Inten-  
363 sif pour la Mer' at Ifremer, Brest, France.

## 364 **Open Research**

365 CTD data were provided through SeaDataNet Pan-European infrastructure for ocean  
366 and marine data management (<https://www.seadatanet.org>), and can be downloaded  
367 as part of the SDC\_ARC\_DATA\_TS\_V2 dataset Due to the large size of simulation  
368 outputs, they are available upon request. A script to reproduce particle advection sim-  
369 ulations can be obtained online (<https://zenodo.org/doi/10.5281/zenodo.3824499>).

**References**

- 370
- 371 Beaird, N., Rhines, P., & Eriksen, C. (2013). Overflow waters at the Iceland–Faroe  
372 Ridge observed in multiyear seaglider surveys. *Journal of Physical Oceanography*,  
373 *43*(11), 2334–2351.
- 374 Becker, J. J., Sandwell, D. T., Smith, W. H. F., Braud, J., Binder, B., Depner, J.,  
375 ... Weatherall, P. (2009, November). Global Bathymetry and Elevation Data at  
376 30 Arc Seconds Resolution: SRTM30\_plus. *Marine Geodesy*, *32*(4), 355–371. doi:  
377 10.1080/01490410903297766
- 378 Bianchi, G. G., & McCave, I. N. (1999). Holocene periodicity in North Atlantic cli-  
379 mate and deep-ocean flow south of Iceland. *Nature*, *397*(6719), 515–517.
- 380 Bosse, A., Testor, P., Houpert, L., Damien, P., Prieur, L., Hayes, D., ... Mortier, L.  
381 (2016, October). Scales and dynamics of Submesoscale Coherent Vortices formed  
382 by deep convection in the northwestern Mediterranean Sea: Vortices in the NW  
383 Mediterranean Sea. *Journal of Geophysical Research: Oceans*, *121*(10), 7716–7742.  
384 doi: 10.1002/2016JC012144
- 385 Bowles, F. A., & Jahn, W. H. (1983). Geological/geophysical observations and in-  
386 ferred bottom-current flow: South flank Iceland—Faeroe Ridge. *Marine Geology*,  
387 *52*(3-4), 159–185.
- 388 Brakstad, A., Gebbie, G., Våge, K., Jeansson, E., & Ólafsdóttir, S. R. (2023).  
389 Formation and pathways of dense water in the Nordic Seas based on a regional  
390 inversion. *Progress in Oceanography*, *212*, 102981.
- 391 Brakstad, A., Våge, K., Ólafsdóttir, S. R., Jeansson, E., & Gebbie, G. (2023). Hy-  
392 drographic and geochemical observations in the nordic seas between 1950 and  
393 2019. , 102981. doi: 10.21335/NMDC-1271328906
- 394 Brink, K. H., & Lentz, S. J. (2010). Buoyancy arrest and bottom ekman transport.  
395 part i: Steady flow. *Journal of Physical Oceanography*, *40*(4), 621–635.
- 396 Buckley, M. W., & Marshall, J. (2016). Observations, inferences, and mechanisms  
397 of the Atlantic Meridional Overturning Circulation: A review. *Reviews of Geo-*  
398 *physics*, *54*(1), 5–63.
- 399 Buhl-Mortensen, L., Olafsdottir, S. H., Buhl-Mortensen, P., Burgos, J. M., & Rag-  
400 narsson, S. A. (2015). Distribution of nine cold-water coral species (Scleractinia  
401 and Gorgonacea) in the cold temperate North Atlantic: effects of bathymetry and  
402 hydrography. *Hydrobiologia*, *759*, 39–61.

- 403 Carton, J. A., & Giese, B. S. (2008, August). A Reanalysis of Ocean Climate Us-  
 404 ing Simple Ocean Data Assimilation (SODA). *Monthly Weather Review*, *136*(8),  
 405 2999–3017. doi: 10.1175/2007MWR1978.1
- 406 Chafik, L., & Rossby, T. (2019). Volume, heat, and freshwater divergences in the  
 407 subpolar North Atlantic suggest the Nordic Seas as key to the state of the merid-  
 408 ional overturning circulation. *Geophysical Research Letters*, *46*(9), 4799–4808.
- 409 Daniault, N., Mercier, H., Lherminier, P., Sarafanov, A., Falina, A., Zunino, P., . . .  
 410 others (2016). The northern North Atlantic Ocean mean circulation in the early  
 411 21st century. *Progress in Oceanography*, *146*, 142–158.
- 412 de Lavergne, C., Groeskamp, S., Zika, J., & Johnson, H. L. (2022). The role of mix-  
 413 ing in the large-scale ocean circulation. *Ocean mixing*, 35–63.
- 414 de Marez, C., Carton, X., Corréard, S., l’Hégaret, P., & Morvan, M. (2020). Obser-  
 415 vations of a deep submesoscale cyclonic vortex in the arabian sea. *Geophysical Re-*  
 416 *search Letters*, *47*(13), e2020GL087881.
- 417 de Marez, C., Le Corre, M., & Gula, J. (2021). The influence of merger and convec-  
 418 tion on an anticyclonic eddy trapped in a bowl. *Ocean Modelling*, *167*, 101874.
- 419 Dee, D. P., Uppala, S. M., Simmons, A. J., Berrisford, P., Poli, P., Kobayashi, S.,  
 420 . . . Vitart, F. (2011, April). The ERA-Interim reanalysis: configuration and  
 421 performance of the data assimilation system. *Quarterly Journal of the Royal*  
 422 *Meteorological Society*, *137*(656), 553–597. doi: 10.1002/qj.828
- 423 Delandmeter, P., & van Sebille, E. (2019, August). The Parcels v2.0 Lagrangian  
 424 framework: new field interpolation schemes. *Geoscientific Model Development*,  
 425 *12*(8), 3571–3584. doi: 10.5194/gmd-12-3571-2019
- 426 de Marez, C., & Le Corre, M. (n.d.). Can the earth be flat? A physical oceanogra-  
 427 pher’s perspective.
- 428 Drijfhout, S., Van Oldenborgh, G. J., & Cimadoribus, A. (2012). Is a decline of  
 429 AMOC causing the warming hole above the North Atlantic in observed and mod-  
 430 eled warming patterns? *Journal of Climate*, *25*(24), 8373–8379.
- 431 Ferrari, R., & Wunsch, C. (2009). Ocean circulation kinetic energy: Reservoirs,  
 432 sources, and sinks. *Annual Review of Fluid Mechanics*, *41*, 253–282.
- 433 Gula, J., Blacic, T. M., & Todd, R. E. (2019, March). Submesoscale Coherent Vor-  
 434 tices in the Gulf Stream. *Geophysical Research Letters*, *46*(5), 2704–2714. doi: 10  
 435 .1029/2019GL081919

- 436 Gula, J., Taylor, J., Shcherbina, A., & Mahadevan, A. (2022). Submesoscale pro-  
437 cesses and mixing. In *Ocean mixing* (pp. 181–214). Elsevier.
- 438 Guo, C., Ilicak, M., Fer, I., Darelius, E., & Bentsen, M. (2014). Baroclinic instability  
439 of the Faroe Bank Channel overflow. *Journal of Physical Oceanography*, *44*(10),  
440 2698–2717.
- 441 Hansen, B. (1985). The circulation of the northern part of the Northeast Atlantic.  
442 *Rit. Fisk.*, *9*, 110–126.
- 443 Hansen, B., Húsgarð Larsen, K. M., Hátún, H., & Østerhus, S. (2016). A stable  
444 faroe bank channel overflow 1995–2015. *Ocean Science*, *12*(6), 1205–1220.
- 445 Hansen, B., Larsen, K. M. H., Olsen, S. M., Quadfasel, D., Jochumsen, K., & Øster-  
446 hus, S. (2018). Overflow of cold water across the Iceland–Farø Ridge through the  
447 Western Valley. *Ocean Science*, *14*(4), 871–885.
- 448 Hansen, B., & Østerhus, S. (2000). North atlantic–nordic seas exchanges. *Progress in*  
449 *oceanography*, *45*(2), 109–208.
- 450 Hansen, B., & Østerhus, S. (2007). Faroe bank channel overflow 1995–2005. *Progress*  
451 *in Oceanography*, *75*(4), 817–856.
- 452 Jayne, S. R. (2009). The impact of abyssal mixing parameterizations in an ocean  
453 general circulation model. *Journal of Physical Oceanography*, *39*(7), 1756–1775.
- 454 Klein, P., Hua, B. L., Lapeyre, G., Capet, X., Le Gentil, S., & Sasaki, H. (2008, Au-  
455 gust). Upper Ocean Turbulence from High-Resolution 3D Simulations. *Journal of*  
456 *Physical Oceanography*, *38*(8), 1748–1763.
- 457 Koman, G., Johns, W., Houk, A., Houpert, L., & Li, F. (2022). Circulation and  
458 overturning in the eastern North Atlantic subpolar gyre. *Progress in oceanography*,  
459 *208*, 102884.
- 460 Kostov, Y., Armour, K. C., & Marshall, J. (2014). Impact of the Atlantic meridional  
461 overturning circulation on ocean heat storage and transient climate change. *Geo-*  
462 *physical Research Letters*, *41*(6), 2108–2116.
- 463 LaCasce, J. H., & Groeskamp, S. (2020). Baroclinic modes over rough bathymetry  
464 and the surface deformation radius. *Journal of Physical Oceanography*, *50*(10),  
465 2835–2847.
- 466 Lange, M., & van Sebille, E. (2017, November). Parcels v0.9: prototyping a La-  
467 grangian ocean analysis framework for the petascale age. *Geoscientific Model De-*  
468 *velopment*, *10*(11), 4175–4186. doi: 10.5194/gmd-10-4175-2017

- 469 Le Corre, M., Gula, J., Smilenova, A., & Houper, L. (2019). On the dynamics of a  
470 deep quasi-permanent anticyclonic eddy in the rockall trough. *French Congress of*  
471 *Mechanics*.
- 472 Le Corre, M., Gula, J., & Treguier, A. M. (2019). Barotropic vorticity balance of the  
473 north atlantic subpolar gyre in an eddy-resolving model. *Ocean Science*. doi: 10  
474 .5194/os-2019-114
- 475 Lévy, M., Franks, P. J., & Smith, K. S. (2018). The role of submesoscale currents in  
476 structuring marine ecosystems. *Nature communications*, *9*(1), 4758.
- 477 L'Hégaret, P., Carton, X., Louazel, S., & Boutin, G. (2016, May). Mesoscale eddies  
478 and submesoscale structures of Persian Gulf Water off the Omani coast in spring  
479 2011. *Ocean Science*, *12*(3), 687–701. doi: 10.5194/os-12-687-2016
- 480 Logemann, K., Ólafsson, J., Snorrason, Á., Valdimarsson, H., & Marteinsdóttir, G.  
481 (2013). The circulation of icelandic waters—a modelling study. *Ocean Science*,  
482 *9*(5), 931–955.
- 483 Lozier, M. S., Li, F., Bacon, S., Bahr, F., Bower, A. S., Cunningham, S., . . . others  
484 (2019). A sea change in our view of overturning in the subpolar North Atlantic.  
485 *Science*, *363*(6426), 516–521.
- 486 Marshall, J., Armour, K. C., Scott, J. R., Kostov, Y., Hausmann, U., Ferreira, D.,  
487 . . . Bitz, C. M. (2014). The ocean's role in polar climate change: asymmetric  
488 arctic and antarctic responses to greenhouse gas and ozone forcing. *Philosophi-*  
489 *cal Transactions of the Royal Society A: Mathematical, Physical and Engineering*  
490 *Sciences*, *372*(2019), 20130040.
- 491 McWilliams, J. C. (2019, December). A survey of submesoscale currents. *Geoscience*  
492 *Letters*, *6*(1). doi: 10.1186/s40562-019-0133-3
- 493 Meehl, G. A., Goddard, L., Boer, G., Burgman, R., Branstator, G., Cassou, C., . . .  
494 others (2014). Decadal climate prediction: an update from the trenches. *Bulletin*  
495 *of the American Meteorological Society*, *95*(2), 243–267.
- 496 Meunier, T., Tenreiro, M., Pallàs-Sanz, E., Ochoa, J., Ruiz-Angulo, A., Portela, E.,  
497 . . . Carton, X. (2018, August). Intrathermocline Eddies Embedded Within an  
498 Anticyclonic Vortex Ring. *Geophysical Research Letters*, *45*(15), 7624–7633. doi:  
499 10.1029/2018GL077527
- 500 Mienis, F., Bouma, T., Witbaard, R., Van Oevelen, D., & Duineveld, G. (2019). Ex-  
501 perimental assessment of the effects of coldwater coral patches on water flow. *Ma-*

- 502 *rine Ecology Progress Series*, 609, 101–117.
- 503 Ólafsdóttir, S. R., Danielsen, M., Ólafsdóttir, E., Benoit-Cattin, A., Sliwinski, J., &  
504 Macrandar, A. (2020). Ástand sjávar 2017 og 2018. *Haf-og vatnarannsóknir*.
- 505 Perkins, H., Hopkins, T., Malmberg, S.-A., Poulain, P.-M., & Warn-Varnas, A.  
506 (1998). Oceanographic conditions east of Iceland. *Journal of Geophysical Re-*  
507 *search: Oceans*, 103(C10), 21531–21542.
- 508 Petit, T., Mercier, H., & Thierry, V. (2019). New insight into the formation and evo-  
509 lution of the East Reykjanes Ridge current and Irminger current. *Journal of Geo-*  
510 *physical Research: Oceans*, 124(12), 9171–9189.
- 511 Polzin, K. L., & McDougall, T. J. (2022). Mixing at the ocean’s bottom boundary.  
512 In *Ocean mixing* (pp. 145–180). Elsevier.
- 513 Polzin, K. L., Wang, B., Wang, Z., Thwaites, F., & Williams III, A. J. (2021).  
514 Moored flux and dissipation estimates from the northern deepwater gulf of mexico.  
515 *Fluids*, 6(7), 237.
- 516 Semper, S., Pickart, R. S., Våge, K., Larsen, K. M. H., Hátún, H., & Hansen, B.  
517 (2020). The Iceland-Faroe Slope Jet: a conduit for dense water toward the Faroe  
518 Bank Channel overflow. *Nature communications*, 11(1), 5390.
- 519 Shchepetkin, A. F., & McWilliams, J. C. (2005, January). The regional oceanic  
520 modeling system (ROMS): a split-explicit, free-surface, topography-following-  
521 coordinate oceanic model. *Ocean Modelling*, 9(4), 347–404.
- 522 Shchepetkin, A. F., & McWilliams, J. C. (2011, January). Accurate Boussinesq  
523 oceanic modeling with a practical, “Stiffened” Equation of State. *Ocean Modelling*,  
524 38(1-2), 41–70. doi: 10.1016/j.ocemod.2011.01.010
- 525 Shor, A. N. (1980). *Bottom currents and abyssal sedimentation processes south of*  
526 *iceland* (Doctoral dissertation, Massachusetts Institute of Technology). Retrieved  
527 from <https://dspace.mit.edu/handle/1721.1/58122>
- 528 Shu, Q., Wang, Q., Årthun, M., Wang, S., Song, Z., Zhang, M., & Qiao, F. (2022).  
529 Arctic ocean amplification in a warming climate in cmip6 models. *Science Ad-*  
530 *vances*, 8(30), eabn9755.
- 531 Siegelman, L., Klein, P., Rivière, P., Thompson, A. F., Torres, H. S., Flexas, M., &  
532 Menemenlis, D. (2020). Enhanced upward heat transport at deep submesoscale  
533 ocean fronts. *Nature Geoscience*, 13(1), 50–55.
- 534 Smilenova, A., Gula, J., Le Corre, M., Houpert, L., & Reecht, Y. (n.d.). A persistent

- 535 deep anticyclonic vortex in the rockall trough sustained by anticyclonic vortices  
536 shed from the slope current and wintertime convection.
- 537 Stow, D., & Holbrook, J. (1984). North Atlantic contourites: an overview. *Geological*  
538 *Society, London, Special Publications*, 15(1), 245–256.
- 539 Su, Z., Wang, J., Klein, P., Thompson, A. F., & Menemenlis, D. (2018). Ocean sub-  
540 mesoscales as a key component of the global heat budget. *Nature communications*,  
541 9(1), 775.
- 542 Tsubouchi, T., Våge, K., Hansen, B., Larsen, K. M. H., Østerhus, S., Johnson, C.,  
543 ... Valdimarsson, H. (2021). Increased ocean heat transport into the Nordic Seas  
544 and Arctic Ocean over the period 1993–2016. *Nature Climate Change*, 11(1),  
545 21–26.
- 546 Ullgren, J. E., Fer, I., Darelius, E., & Beaird, N. (2014). Interaction of the Faroe  
547 Bank Channel overflow with Iceland Basin intermediate waters. *Journal of Geo-*  
548 *physical Research: Oceans*, 119(1), 228–240.
- 549 Vic, C., Naveira Garabato, A. C., Green, J. M., Waterhouse, A. F., Zhao, Z., Melet,  
550 A., ... Stephenson, G. R. (2019). Deep-ocean mixing driven by small-scale  
551 internal tides. *Nature communications*, 10(1), 2099.
- 552 Wang, L., Gula, J., Collin, J., & Mémerly, L. (2022). Effects of Mesoscale Dynam-  
553 ics on the Path of Fast-Sinking Particles to the Deep Ocean: A Modeling Study.  
554 *Journal Of Geophysical Research-oceans*, 127(7).
- 555 Winton, M., Griffies, S. M., Samuels, B. L., Sarmiento, J. L., & Frölicher, T. L.  
556 (2013). Connecting changing ocean circulation with changing climate. *Journal of*  
557 *climate*, 26(7), 2268–2278.
- 558 Zhao, J., Bower, A., Yang, J., Lin, X., & Penny Holliday, N. (2018). Meridional  
559 heat transport variability induced by mesoscale processes in the subpolar North  
560 Atlantic. *Nature communications*, 9(1), 1124.
- 561 Zhong, Y., & Bracco, A. (2013). Submesoscale impacts on horizontal and verti-  
562 cal transport in the gulf of mexico. *Journal of Geophysical Research: Oceans*,  
563 118(10), 5651–5668.
- 564 Zou, S., Lozier, S., Zenk, W., Bower, A., & Johns, W. (2017). Observed and mod-  
565 eled pathways of the Iceland Scotland Overflow Water in the eastern North At-  
566 lantic. *Progress in Oceanography*, 159, 211–222.